Earthquake geology of the Mondy fault (SW Baikal Rift, Siberia)

A V Arzhannikova, S G Arzhannikov, A A Chebotarev, A S Yakhnenko, Jean-François Ritz

Journal of Asian Earth Sciences 248 (2023) 105614

Contents lists available at ScienceDirect

Journal of Asian Earth Sciences

journal homepage: www.elsevier.com/locate/jseaes

Earthquake geology of the Mondy fault (SW Baikal Rift, Siberia)

A.V. Arzhannikova [a,b,*], S.G. Arzhannikov [a], J.-F. Ritz [c], A.A. Chebotarev [a], A.S. Yakhnenko [d,e]

[a] Institute of the Earth Crust, Russian Acad. of Sciences, Siberian Branch, Irkutsk, Russia
[b] Geological Institute, Russian Acad. of Sciences, Moscow, Russia
[c] Géosciences Montpellier, CNRS, Université de Montpellier, UMR 5243, France
[d] Limnological Institute, Russian Acad. of Sciences, Siberian Branch, Irkutsk, Russia
[e] Joint Institute for Nuclear Research, Dubna, Russia

ARTICLE INFO

Keywords:
Morphotectonics
Paleoseismology
Active fault
Tunka Basin
Baikal Rift

ABSTRACT

The Mondy Fault is a 90 km long E-W trending active structure belonging to the southwestern part of the Baikal rift system, connecting the Tunka depression to the East to the Hovsgol rift to the West. The fault is well expressed in the morphology and formed during the Neogene within a transtensional strain regime (left-lateral + normal) contemporaneously with the opening of the Baikal Rift. On April 4th, 1950, the fault produced a large earthquake with a moment magnitude of Mw 6.9, and a left-lateral focal mechanism. Along with other structures of the Tunka depression such as the Tunka and Sayan faults, it represents a seismic hazard for the cities in the region as the Irkutsk agglomeration (1 million people). To characterize its potential activity, we combined morphotectonic and paleoseismological investigations at two sites along the eastern and western parts of the fault, respectively. Our study shows that cumulative left-lateral displacements are associated with a strong reverse component. This indicating that the previous Neogene normal vertical component has been reversed, consistently with the inversion of the tectonic regime observed within the SW Baikal Rift region in the Late Pleistocene-Holocene. We estimated the slip rate along the fault to be 0.9–1.5 mm/yr over the last ~ 13 ka, and identified four large surface-rupturing events with minimum magnitude of 7.4 separated by an average recurrence interval of 3.9–4.6 ka.

1. Introduction

The Mondy Fault is a 90 km long N095°E trending left-lateral strike-slip fault located within the southwestern region of the Baikal Rift. It connects the EW trending Tunka depression to the East with the NS trending Hovsgol rift. Within the transition zone between transpression in Mongolia and extension in Baikal, the Mondy fault region has experienced transpressional deformations since at least the Late Pleistocene. This regime postdates the transtensional that was active since the Oligocene (Parfeevets and San'kov, 2006; Larroque et al., 2001). This recent change in strain regime appears as a regional phenomenon as it is also observed within the eastern part of the Tunka depression. Compared to the faults that controlled the recent (Late Pleistocence-Holocene) to present tectonics within the Tunka depression which have been the subject of several works in morphotectonics and paleoseismology (McCalpin and Khromovskikh, 1995; Chipizubov, Smekalin, 1999; Chipizubov et al., 2003; Smekalin et al., 2013; Arzhannikova et al., 2018; Ritz et al., 2018), the Mondy Fault remains poorly studied. However, it represents in the same way as the Tunka and Sayan faults, one of the main seismogenic structures on the SW Baikal Rift region. The fault produced a Mw 6.9 earthquake on April 4th, 1950. Several discordant focal mechanisms have been proposed for that event; the best fitting mechanism showed a nodal plane orientated close to E–W associated with right-lateral movement (Doser, 1991). Reassessment of the focal mechanism solution using a new approach in source inversion showed a left-lateral strike-slip displacement along the E-W plan, corresponding to the strike of the fault (Fig. 1) (Delouis et al., 2002). Several attempts were carried out to map surface ruptures, determine Late Pleistocene–Holocene fault kinematics, and date paleoearthquakes (Arjannikova et al., 2004; Treskov, Florensov, 2006; Lunina et al., 2015; 2016), but neither slip rates nor the recurrence interval of surface-rupturing events have been determined yet. Besides, the Late Pleistocene–Holocene fault kinematics, in terms of the vertical component, remains debatable (Arzhannikova et al., 2003; Arjannikova et al., 2004; Lunina et al., 2016).

In this paper, we present the results of a morphotectonic and

* Corresponding author.
E-mail address: arzhan@crust.irk.ru (A.V. Arzhannikova).

https://doi.org/10.1016/j.jseaes.2023.105614
Received 1 November 2022; Received in revised form 20 January 2023; Accepted 8 March 2023
Available online 14 March 2023

paleoseismic study carried out along two segments of the Mondy Fault. They allow characterizing the present kinematics of the fault and constraining the age and magnitude of the four-last surface-rupturing events. Combined with data from previous studies carried out along the Tunka and Sayan faults, our results allow discussing the distribution in space and time of past large earthquakes within the Baikal Rift southwestern region.

2. Tectonic setting

Baikal Rift is the largest Cenozoic continental rift in Asia, which developed along the boundary between the Siberian Craton and the Amurian Plate. The crustal and lithospheric structure along this boundary is complex, resulting from a series of collision and rifting events that repeatedly occurred before the Baikal rifting from the Paleoproterozoic to the Cretaceous (see a synthesis of this evolution in Jolivet et al. (2009)). According to GPS data (Calais et al., 2003; Sankov et al., 2009; 2014; Lukhnev et al., 2010), the Amurian Plate is moving southeast of the Siberian Craton at a rate of 3–4 mm/yr (Fig. 1). Seismological data show that the central part of the Baikal Rift is deforming in a pure extensional mode, while its SW part is characterized by a complex interaction between extensive and compressive stresses (Petit et al., 1996; Melnikova et al., 2004; Radziminovich et al., 2013; 2016 Radziminovich, 2021; Liu et al., 2022). Within the Tunka depression, the average seismic moment tensor, calculated from both data on the focal mechanisms and seismic moments of earthquakes shows the predominance of a strike-slip deformation regime, with a contribution of compression more significant than extension (Melnikova et al., 2004). Recent tectonic structures described for the Tunka depression show features characteristic of both the transtensional and transpressional deformation regimes, thus the kinematics of faults is under debate (Larroque et al., 2001; Chipizubov et al., 2003; Arzhannikova et al., 2003; 2007; Arjannikova et al., 2004; Parfeevets, San'kov, 2006; Lunina, Gladkov, 2004; Lunina et al., 2015; 2016; Ritz et al., 2000, 2018). Three active faults control the development of the Tunka depression - the Sayan Fault - in the most eastern part, the Tunka Fault - in the central part, and the Mondy Fault - in the most western part (Fig. 1). All these faults display seismic activity and, together with the south Baikal and Primorsky faults, represent a strong seismic hazard for Irkutsk agglomeration with ~ 1 million inhabitants.

The Tunka depression consists of several basins (from west to east: Mondy, Khoytogol, Turan, Tunka, Tory, Bistraya) separated by interbasin heights (Fig. 2). Morphotectonic studies of these basins indicate that some of them have been reversed during the Pleistocene as shown by their recent uplift (Larroque et al., 2001; Arzhannikova et al., 2003, 2005, 2007; Arjannikova et al., 2004; Jolivet et al., 2013; Shchetnikov, 2017; Arzhannikov et al., 2018). This inversion is also observed within the kinematics of the eastern fault sections of the Tunka and Sayan faults, which control the development of the eastern Tory and Bistraya basins. Since the Neogene, these faults functioned as normal and left-lateral strike-slip faults, controlling the subsidence of the basins. However, during the Late Pleistocene-Holocene, the eastern sections of these faults have seen their vertical component being reversed and become a left lateral-reverse faults (Fig. 2) (Chipizubov and Smekalin, 1999; Chipizubov et al., 2003; Ritz et al., 2018).

This kinematic inversion is also observed within the paleoseismological data in the eastern segments of the Tunka and Sayan faults (Fig. 2). Moreover, age constraints about past surface-rupturing earthquakes suggest that both faults could have ruptured together or during seismic clusters since the past 15 ka, producing Mw7–8 earthquakes separated by ~ 4 kyrs recurrence intervals (Ritz et al., 2018). In contrast, paleoseismological investigations along the central segment of the

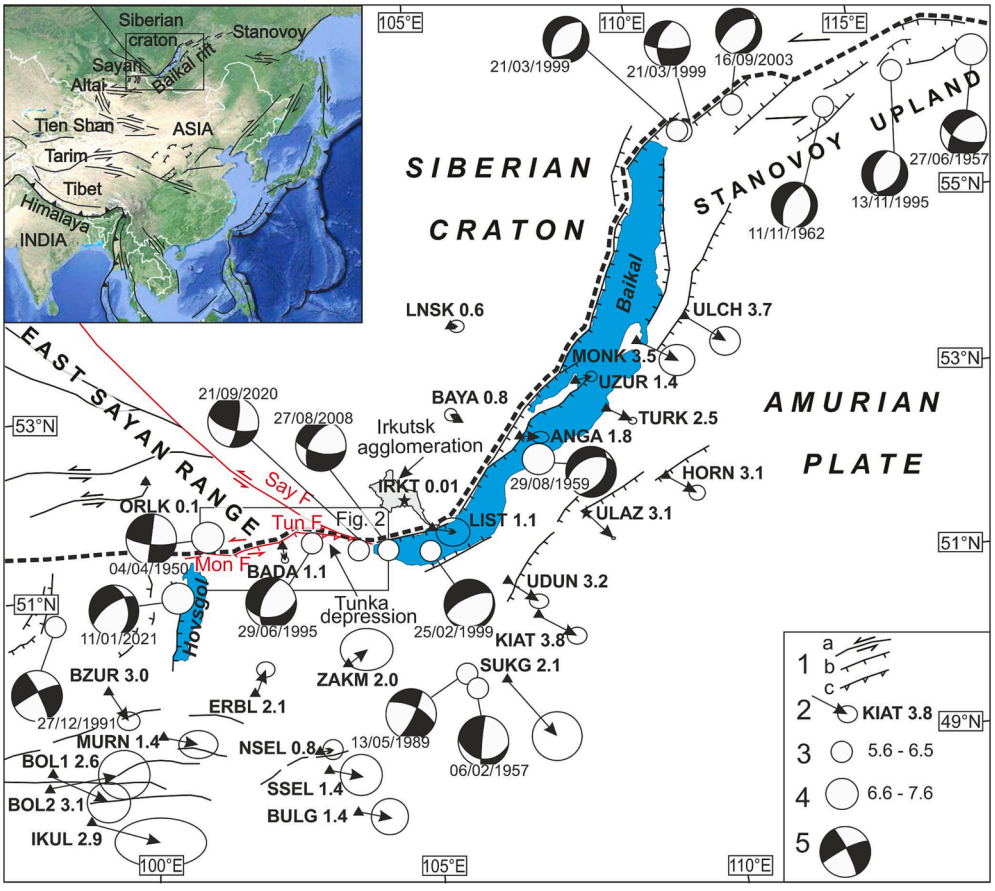

Fig. 1. Map of the main active faults of the Baikal rift area (area enclosed in the rectangle in the insert). The black dashed line indicates the northwestern boundary of the Amurian Plate (after Petit and Fournier, 2005). 1 - Main active faults: a - strike-slip, b - normal; c - reverse; faults discussed in the text are highlighted by red color: Mon F, Tun F and Say F - Mondy, Tunka and Sayan faults, respectively; 2 - GPS horizontal velocities with respect to Eurasia (after Calais et al., 2003; 2006; Sankov et al., 2009; 2014; Lukhnev et al., 2010); 3, 4 - epicenters of the large earthquakes within given magnitude ranges; 5 - focal mechanisms in the lower hemisphere of the earthquakes with M ≥ 5.6 (after Radziminovich et al., 2013; Filippova et al., 2022). Insert - simplified neotectonic map of Asia (modified after Petit and Deverchere, 2006).

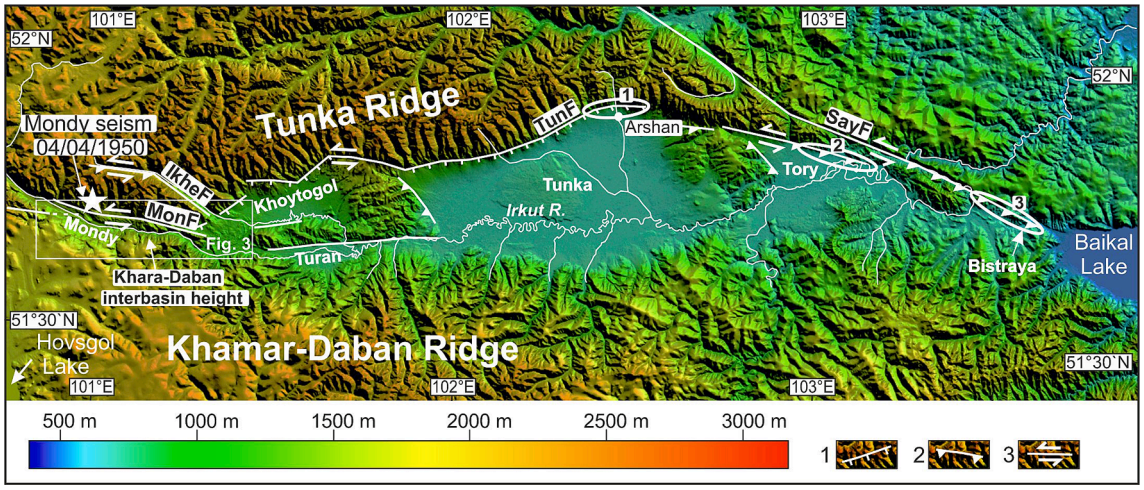

Fig. 2. Digital elevation model of the system of basins of Tunka with main active faults and their recent kinematics (1-normal, 2-reverse, 3-strike-slip): TunF – Tunka, SayF – Sayan, MonF – Mondy, IkheF - Ikhe-Ukhgun faults. White ellipses point out the paleoseismic sites: Arshan (1), Tory (2) and East Sayan (3).

Tunka Fault (Arshan area, Fig. 2), suggest that this part of the fault kept a left lateral normal kinematics during the Late Pleistocene-Holocene, with recurrence interval of strong earthquakes comprised between 2.8 and 3.4 ka (McCalpin and Khromovskikh, 1995; Chipizubov et al., 2003; Smekalin et al., 2013). Ritz et al. (2018) estimated a left-lateral late Pleistocene–Holocene slip rate comprised between 1.3 and 3.9 mm/year for the Sayan Fault. Arzhannikova et al. (2018) and Chebotarev et al. (2021) estimated a vertical slip rate of 0.9 mm/yr and a horizontal slip rate of 1.5 mm/yr along the central segment of the Tunka Fault.

The Mondy Fault was first interpreted as corresponding to the westwards extension of a fault zone running along the southern border of the Tunka depression from the Lake Baikal to the Mondy Basin (Lukina, 1989). However, recent morphotectonic and stratigraphic studies along the southern border of the Tunka depression, at the

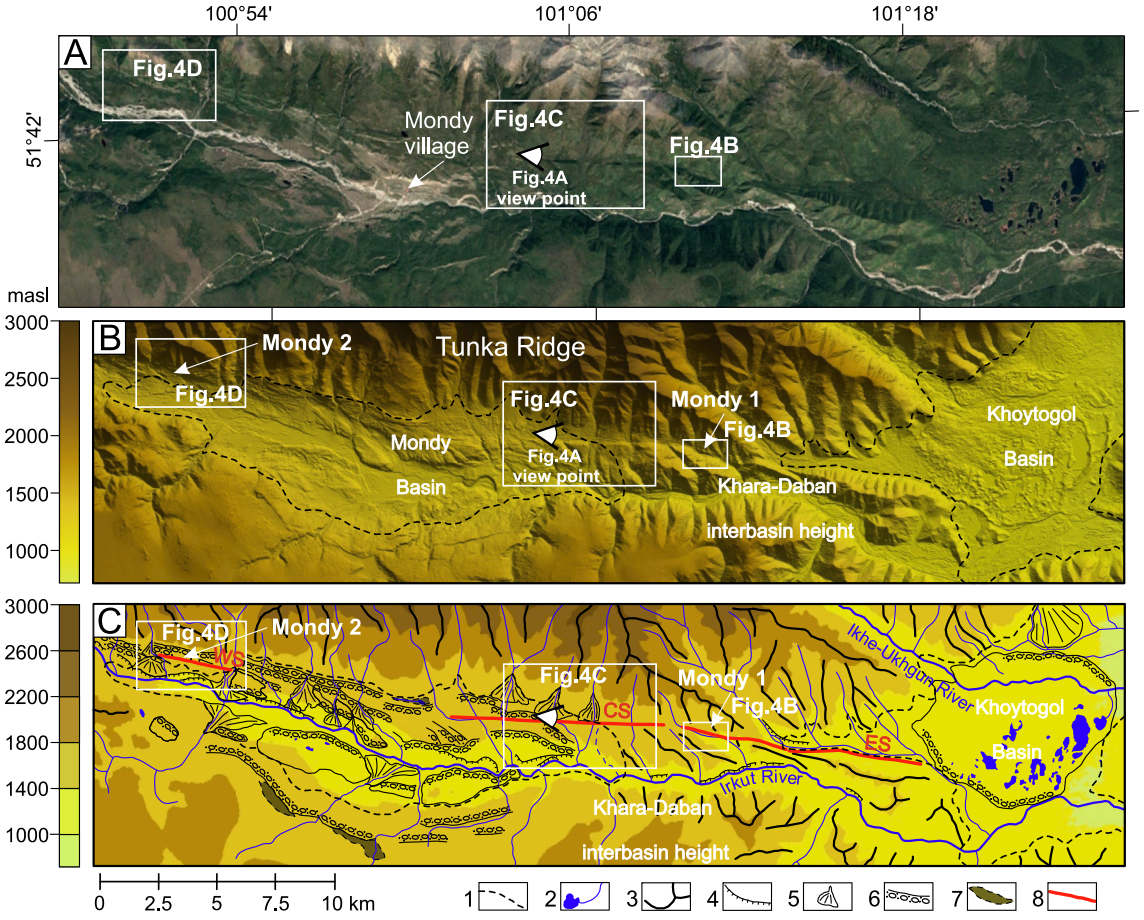

Fig. 3. The Mondy fault area (map area in Fig. 2). (A) Google Earth Landsat image, (B) TanDEM-X 12-m digital elevation model and (C) geomorphological interpretation. 1 - Quaternary deposits within Mondy and Khoytogol basins, 2 - thermokarst lakes and rivers, 3 - crest lines, 4 - alluvial terrace risers, 5 - alluvial fans, 6 - moraines, 7 - kame tarraces, 8 - surficial traces of the Mondy Fault (ES, CS and WS - eastern, central and western segments, respectively).

foothills of the Khamar-Daban Ridge, did not reveal signs of Late Quaternary tectonic deformations (Arzhannikova et al., 2020). On the other hand, the Mondy Fault is well expressed in the morphology along the northern boundary of the Mondy Basin and within the Khara-Daban interbasin height (Fig. 2), and defines a 90 km long E–W-trending left-lateral strike-slip fault connecting the Tunka depression to the Hovsgol rift to the West.

While its left-lateral strike-slip kinematics is unambiguous, with notably obvious offset drainages that can be observed along the fault, there is no consensus regarding the vertical component along the Mondy Fault. Arzhannikova et al. (2003) and Arjannikova et al. (2004) interpreted a reverse vertical component from the occurrence of a counter-slope scarp observed within the eastern part of the fault, combined also with evidences of reverse faulting along the Ikhe-Ukhgun Fault (see Fig. 2 for location). This interpretation is consistent with the solutions of focal mechanisms in the western part of the Tunka depression, which indicate a transpressional regime of deformation (Arzhannikova et al., 2007; Radziminovich, 2021). However, Lunina et al. (2016) interpreted normal fault displacements affecting sub-surface horizons within ground penetrating radar profiles performed across the Mondy fault zone within the Khara-Daban interbasin height.

3. Analyzing the morphotectonics and paleoseismology of the Mondy fault

To clarify the issue of the kinematics along the Mondy Fault and characterize its seismic behavior, we carried out detailed morphotectonic and paleoseismological investigations at two sites with evidence for young displacements, Mondy 1 and 2 (Fig. 3). The eastern one (Mondy 1) is located within the Khara-Daban interbasin height, and the western one (Mondy 2) - within the western part of the Mondy Basin. Using a total station theodolite, we constructed digital elevation models of the two sites that allowed the reconstruction of the fault morphology and kinematics. These DEM allowed also targeting paleoseismic sites where we opened trenches to study surface ruptures in recent deposits.

Fig. 3C shows a detailed geomorphological map of the Mondy Fault built up from the analysis and the interpretation of Google Earth Landsat, Maxar and Bing satellites images and TanDEM-X digital elevation models with 12 m resolution. The Mondy eastern fault segment starts within the western part of the Khoytogol Basin where a large terminal moraine associated with the glacier that descended from the Ikhe-Ukhgun Valley is observed. Radiocarbon dates of samples collected from thermokarst lake deposits in the moraine yielded an age of ~ 11 to ~ 7 ka (Larin, 2019). No tectonic displacements are observed in the moraine deposits, which indicate that the Holocene rupturing along the Mondy Fault does not propagate east of the Khara-Daban interbasin height.

In the central part of the studied area, the Irkut River incised into the Khara-Daban interbasin height, and formed a series of terraces clearly visible in the valley when it widens. Further west, the Mondy Basin defines a large alluvial valley which origin is associated to the glacial processes. There are lateral moraines, kame terraces and thermokarst lakes along the slopes and in the bottom of the Mondy Basin (Fig. 3). Geomorphological and geochronological studies provided evidence for extensive MIS 2 glacier advances into the Mondy Basin. In situ ^{10}Be exposure dates of boulders on the terminal moraines yielded a mean age of ~ 14 ka (Arzhannikov et al., 2015). The Irkut River and its tributaries incise into glacial deposits. Radiocarbon dates of abandoned alluvial terraces allowed estimating a Holocene incision rate of 1.5–1.6 mm/yr (Maksimov, 1965; Arjannikova et al., 2004).

The Mondy Fault is expressed in the morphology by a upslope, northward-facing scarp in the southern slope of the Tunka Ridge (Fig. 4A, see Fig. 3B for location). The fault is subdivided into three segments with a difference both in strike and expression in the

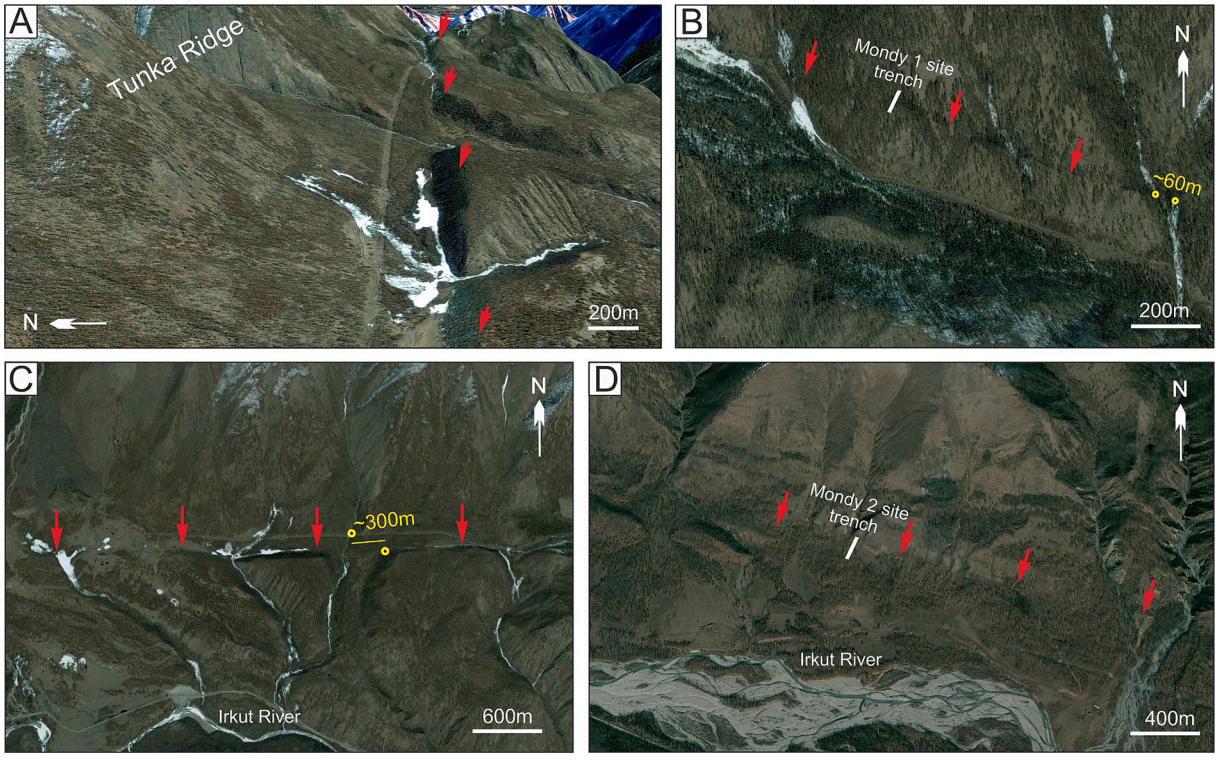

Fig. 4. Satellite view of the details of the morphology of the Mondy Fault. (A) Google Earth Bing satellite image showing the upstream-facing scarp in the southern slope of the Tunka Ridge along the fault. (B) Maxar satellite image showing the youngest surface deformations along the eastern segment of the Mondy Fault (Mondy 1 site). (C) Landsat satellite image showing cumulative long-term displacement along the central segment of the Mondy Fault. (D) Maxar satellite image showing the youngest surface deformations along the western segment of the Mondy Fault (Mondy 2 site). Red arrows indicate the upstream-facing tectonic scarp. Yellow circles indicate the piercing points with horizontal displacement amplitude.

morphology. The eastern segment N100°E trending, 10.7 km long, extends from N51°40.109, E101°18.230 to N51°41.161, E101°8.601 along the northern edge of the Khara-Daban interbasin height (Fig. 3C). Several streams abut against the scarp and are left-laterally shifted. The smallest observed displacement is 10–15 m, while the largest one reaches ~ 60 m, (Mondy 1 site, Fig. 4B, see Fig. 3B for location). The central segment, N093°E trending, 10 km long, extends from N51°41.161, E101°8.601 to N51°41.474, E101°0.209 between the Khara-Daban interbasin height and Tunka Ridge to the east and along the northern side of the Mondy Basin to the west (Fig. 3C). Large upslope-facing scarp and blocked drainage forming alluvial fans upstream the fault scarp indicate a long-term uplift component of the southern hanging wall. Along this segment, we observe left-lateral displacement within offset rivers reaching 300 m (Fig. 4C, see Fig. 3B for location). No recent (and smaller) displacement was found along this segment. The western segment, N105°E, 3.2 km long, extends from N51°42.720, E100°52.770 to N51°43.062, E100°50.036 along the northern side of the western Mondy Basin (Fig. 3C). Young surface deformations well preserved in morphology are observed, such as upslope-facing scarps and left-laterally offset streams with amplitudes of a few meters (Mondy 2 site, Fig. 4D, see Fig. 3B for location).

3.1. Mondy 1 site (eastern segment)

3.1.1. Morphotectonic analysis

The Mondy 1 site is located along the N100°E trending eastern segment of the Mondy Fault. It corresponds to a left-laterally offset shutter ridge with a clear counter-slope scarp at its northern foothills indicating an additional vertical component (Fig. 4B and 5A). To analyze the kinematics of the fault, we surveyed the area (100 × 100 m^2) with an optical station and build up a digital elevation model (Fig. 6A). To estimate the amplitude of the horizontal displacement, piercing lines were drawn on both sides of the displaced ridge. "Piercing lines" correspond to continuous lines sketching the main directions of displaced morphological markers (e.g. shifted creeks, thalwegs axes, top lines of risers) that can be well-fitted on both sides of the fault. The morphotectonic reconstruction of the horizontal component before the left-lateral displacement is shown in Fig. 6B. It allows estimating a cumulative horizontal left-lateral displacement of 14 ± 1.4 m.

We then estimated the cumulative vertical displacement from a topographic profile A-Á crossing the fault scarp before the horizontal shifting in the place where we opened the trench, assuming it was defining a straight line (Fig. 6 B,C). We used the location and the dip angle (75°S) of the main fault (F6) observed in trench (see below) to precisely calculate the amplitude of the vertical component projected on the fault plane according to the axis defined by the piercing line slope (see Nazari et al., 2009 for further detailed explanation). We obtained a value of 13.5 ± 1.3 m (Fig. 6C). We assume a surface offset error of about 10%, including the error in measuring the horizontal and vertical displacements and oblique location of the profiles relative to the fault scarp.

Assuming that the horizontal and vertical finite displacements have the same age (in other word assuming that the shifted left-laterally offset shutter ridge corresponds to an isochronous marker in its 3 dimensions), we calculated a cumulative left-lateral-reverse slip of 19.5 ± 2 m (Fig. 6D) from the cumulative horizontal and vertical components.

3.1.2. Paleoseismological analysis

At the foot of the north-facing counter-slope scarp (51°40.958N; 101°9.996E), we opened by hand a 10 m long, 2.5 m deep trench (Fig. 5, see Fig. 4B for location). Table 1 shows the stratigraphic description of the different units exposed in the trench.

Both trench walls show intense deformation affecting weathered bedrock and silty-clayey trapped colluvium units (Fig. 7). The deposits have undergone plicative and disjunctive deformations. In the central part of the trench, units 45 and 50 form a southwards overturned anticline. The fold axis strikes N100°E parallel to the fault scarp. We consider disjunctive deformations as ruptures with vertical displacement amplitudes up to 0.5 m, fissures, and a 1.5–1.9 m thick vertical zone of intense crushing (Unit 70), which we interpret as the main fault zone. Inside this main fault zone, we observed a system of fissures, dipping steeply southward, filled with organic material. We sampled paleosoils and charcoals from different units for radiocarbon dating (Table 2). Age constraints combined with the analysis of the deformations affecting the units allow interpreting four surface-rupturing events that occurred during the past ~ 13 ka. (Fig. 7). Note, that we did not consider the age 5036–5290 yrs BP (sample MF-19–1) since it is not in stratigraphic order.

The most recent event (MRE, event horizon 1) occurred after the deposition of unit 15, which radiocarbon age is 1054–1184 yrs BP (sample MF-19–11) (Fig. 7). The fault F1 cuts through units 40 and 15, and is overlain by modern soil unit 10. Perhaps this event corresponds to the Mondy earthquake of 1950, but this question remains opened since we could not determine an upper limit for this MRE.

The penultimate event (PE, event horizon 2) occurred after the deposition of unit 20 (Fig. 7). It is observed along the faults F2 and F3 (the latter showing a vertical offset component of ~ 0.5 m), which are sealed by the colluvial wedge unit 18 (F3) and the organic-rich sandy-gravelly unit 15 (F2). A burnt root from a tree that grew in the colluvial wedge yielded an age of 1291–1362 years BP (sample MF-19–8), which defines the minimum age of the PE. Its maximum age is determined by the radiocarbon age (i.e. 5324–5579 years BP) obtained for the underlying unit 40 (sample MF-19–5 in Unit 40). According to these age constraints, the PE occurred between 1291 and 5579 cal. yrs BP.

The pre-penultimate event (PPE, event horizon 3 (Fig. 7)) corresponds to the plicative deformation affecting units 50 and 45 (and

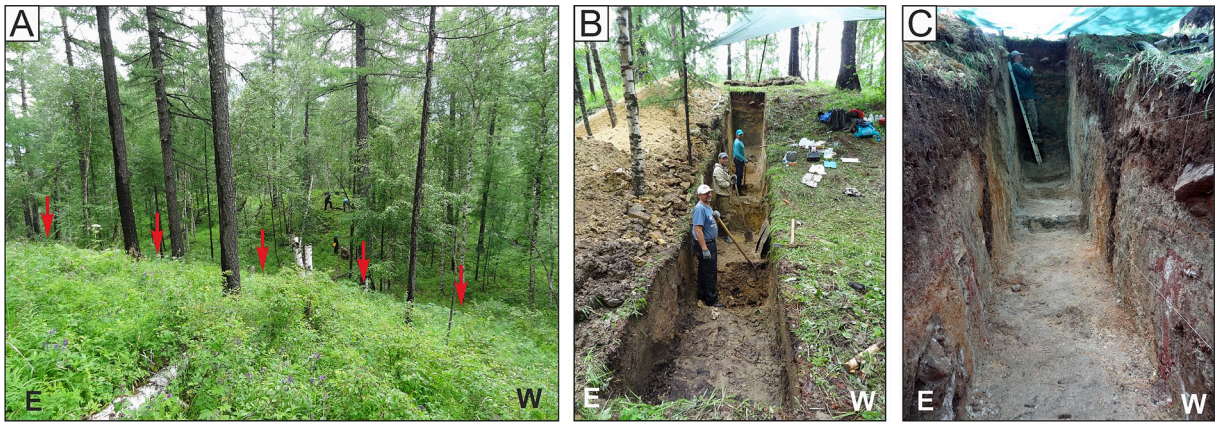

Fig. 5. Field photographs of the left-laterally offset shutter ridge (red arrows indicate the fault trace) (A) and view of the trench (B,C) opened at site Mondy 1.

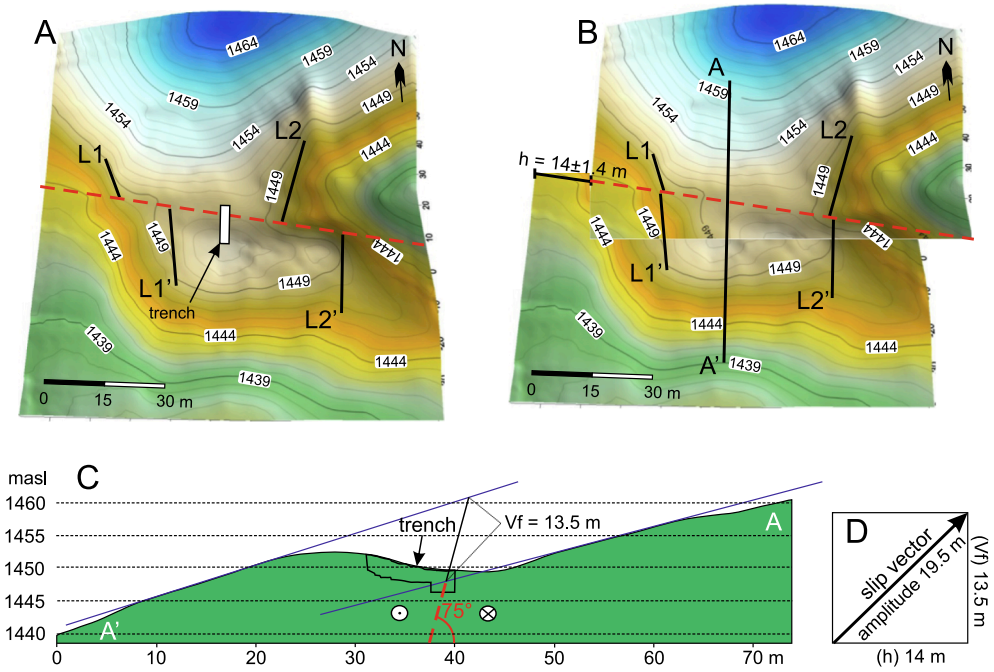

Fig. 6. Digital elevation model (from 1457 topographic points) of the shutter ridge at site Mondy 1 (A) and horizontal component reconstruction before left-lateral displacement (B) from piercing lines (L1-L1′ and L2-L2′). The isolines indicate the absolute height above sea level in meters (masl). (C) Topograpic profile A-A', reconstructed taking into account the horizontal displacement. The Mondy Fault is shown by the red dashed line. (D) Determination of the displacement amplitude along the slip vector. h - horizontal offset, Vf - vertical component projected on the fault plane according to the axis defined by the slope of topographic ridge.

Table 1
Stratigraphic descriptions for units logged in the trench at site Mondy 1.

Unit	Description of stratigraphy
10	black organic soil with unsorted gravels up to 1 cm
15	light brown organic-rich sandy-gravelly unit
16	white-beige kaolinite unit with unsorted gravels up to 20 cm
18	brown clast-supported unit with sandy matrix, fragments of kaolinite and angular to sub-rounded gravels up to 12 cm; unit interpreted as a colluvial wedge
20	white-beige kaolinite unit; re-deposited products of the weathered rock
30	a burnt root from a tree that grew in the colluvial wedge
40	brown silty unit with matrix rich in humus, charcoals and rock fragments up to 34 cm; unit is affected by ruptures filled with humus
42	gray silty unit filling the depression above the fault zone, with small humus lenses
45	humus-rich unit with weathered rock clasts folded with unit 50
50	predominantly red kaolin-rich weathered rock, locally white and purple
60	predominantly blue-green weathered rock
70	gray silt unit with clasts up to 35 cm filling the main fault zone

probably unit 60 in the southern part of the trench), interpreted as contemporaneous of the faulting along F4 and probably also along the main N100°E trending, 75° south-dipping fault F6 (although there is no direct evidence to say so, but only the reasonable deduction that the compressive deformation observed in the trench and at the origin of the counter-slope scarp observed in the morphology is necessarily controlled by this main south-dipping fault). The age of the PPE is bracketed between 9001 and 9274 years BP (sample MF-19–6), the age of the paleosoil unit 45, and 7580–7698 years BP (sample MF-19–3), the age of unit 42 against which fault F6 terminates.

An earlier event (EE, event horizon 4, Fig. 7) is interpreted along fault F6 cutting through the crushed unit 70 in which a charcoal-rich paleosoil is sheared. Sample (MF-19–2) collected in the sheared unit yielded an age of 12760–13009 cal. years BP predating this EE. Since the upper part of unit 70 is eroded and the nearest date from the overlapping unit 42 postdates the PPE, the lower age limit for the PPE (9001–9274 years BP) was taken as the upper age limit for EE. Thus, we bracketed the EE between 13,003 and 9001 cal. years BP.

3.1.3. *Maximum slip rate, average magnitude and mean recurrence intervals of earthquakes*

Combining data obtained from our morphotectonic and paleoseismological analyses allow estimating the maximum slip rate along the eastern segment of the Mondy Fault, and estimating the average recurrence and magnitude of past surface-rupturing earthquakes. We cannot be totally certain that the number of events observed in the trench is responsible for the observed cumulated slip at the surface. However, given that the deepest and oldest units observed in the trench correspond to bedrock units, it is reasonable to consider that the trapped sediments above these bedrock units are associated with the deformation recorded in the morphology. We cannot preclude that some erosional processes occurred and would have removed the stratigraphic signatures of additional events - especially if they were smaller in magnitude -, but this scenario seems difficult to imagine, at least for large events, given the pond-shaped morphology of the trapping area behind the counter-slope scarp. Therefore, considering that the ~ 19.5 m cumulative slip is the result of at least four events that occurred during the past 13 ka allows estimating a maximum slip rate of 1.5 mm/yr, with horizontal and vertical components of 1.1 and 1.0 mm/yr, respectively. It also allows estimating an average slip per event of 4.9 ± 0.5 m, yielding a mean Moment magnitude of earthquake of M_w 7.5 after Wells and Coppersmith (1994)'s statistical functions. The results show that the M_w6.9 1950 Mondy event was probably not associated with a surface rupture, at least in this studied site.

Our morphotectonic analysis at the site Mondy 1 suggests that the ~ 19.5 m cumulative displacement corresponds to the four surface rupturing events identified in the trench, which occurred during the last 13 ka. Given that we do not know when occurred the last event we calculate a mean recurrence interval comprised between 3.9 and 4.3 ka.

3.2. *Mondy 2 site (western segment)*

3.2.1. *Morphotectonic analysis*

The western segment of the Mondy Fault (see Fig. 3C and 4D) is 3.2 km long and represents an upslope-facing scarp with a N105°E direction on the southern slope of the Tunka Ridge (Fig. 8A). Small valleys and streams are left-laterally displaced by the fault with an amplitude of a few meters. To analyze the kinematics of the eastern segment of the

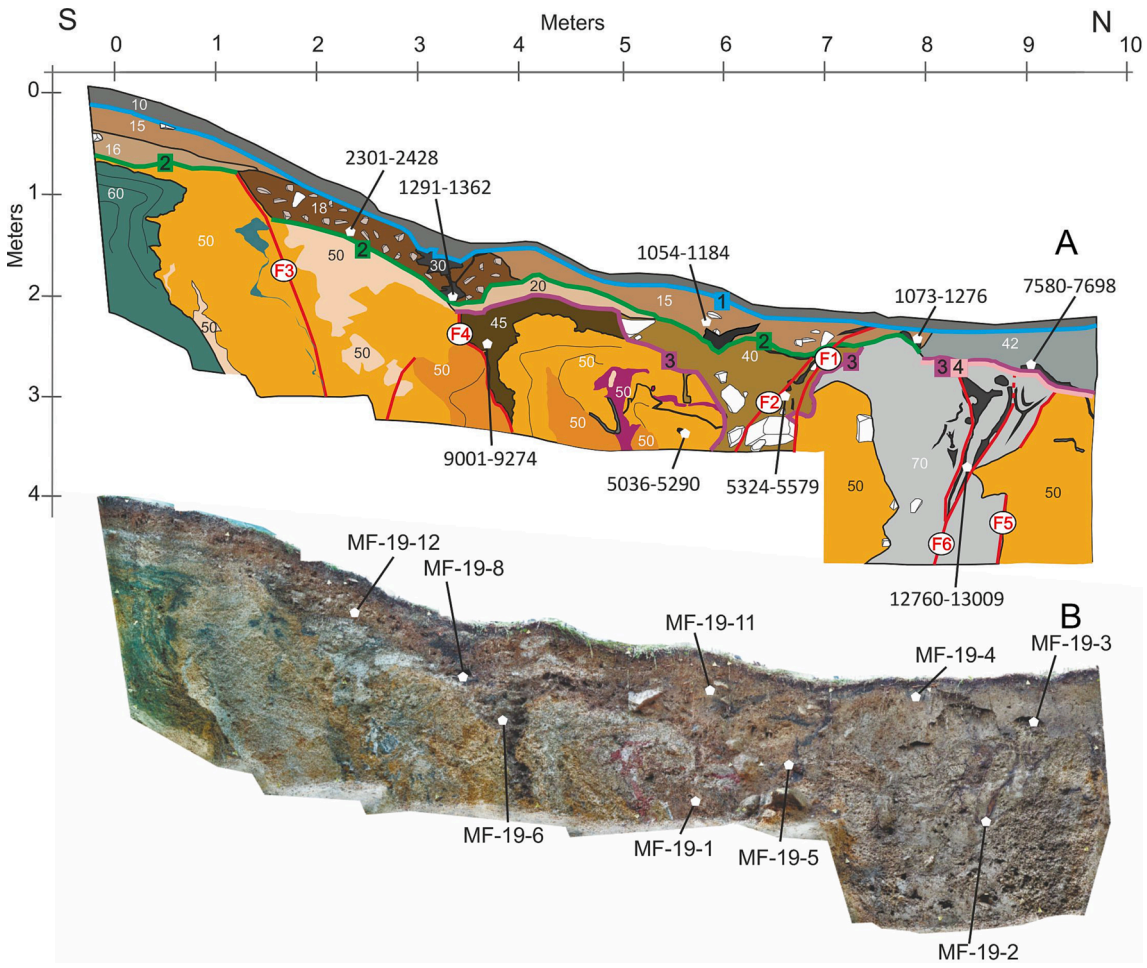

Fig. 7. Log (A) and photomosaic (B) of the western wall of the trench dug in site Mondy 1 (Units are described in Table 1). White pentagons show the location of samples collected for radiocarbon analysis (black numbers correspond to calibrated years BP in the log, and to samples numbers in the mosaic). Red lines correspond to faults (F1-F6). Other bold colored lines define event horizons (1–4).

Table 2
Calculated dates from radiocarbon analysis of paleosoils and charcoals collected in the trench at site Mondy 1. Dendrochronologically calibrated calendar ages were calculated using CALIB 8.2 (Stuiver et al., 2021).

Sample name	Unit number	Lab. no.	^{14}C age year BP	Calibrated age, year BP (2σ)
MF-19–1	50	SacA-59681	4480 ± 30	5036–5290
MF-19–2	70	Poz-118284	10970 ± 60	12760–13009
MF-19–3	42	SacA-59682	6815 ± 35	7580–7698
MF-19–4	15	Poz-118285	1250 ± 30	1073–1276
MF-19–5	40	Poz-118487	4725 ± 35	5324–5579
MF-19–6	45	Poz-118488	8160 ± 50	9001–9274
MF-19–8	30	SacA-59683	1425 ± 30	1291–1362
MF-19–11	15	Poz-118485	1195 ± 30	1054–1184
MF-19–12	18	Poz-118286	2320 ± 35	2301–2428

Mondy Fault and determine the horizontal and vertical displacement amplitudes, a detailed topographic mapping was carried out in an area of 110 × 80 m^2 (Fig. 9A).

To determine the amplitude of the horizontal offset, we considered the piercing lines corresponding to 3 successive displacements: 1) a small creek and the top line of its westward riser (lines L1-L1′ and L2-L2′, respectively), 2) the top line of an older riser (L3-L3′), and 3) the previous position of the downstream part of the L3 riser (L3-L3″) together with the top line of another riser (L4-L4′) (Fig. 9A). Restoration of the original position of these piercing lines yields mean horizontal offset of 3.5 ± 0.3 m (L1-L1́and L2-L2́) (Fig. 9B), 7 ± 0.7 m (L3-L3′) (Fig. 9C) and 10.5 ± 1 m (L3-L3″ and L4-L4′) (Fig. 9D).

To determine the vertical displacement amplitude, we performed topographic profiles along the different piercing lines when restored (Fig. 9 E). As in the site Mondy 1, we used the location and the mean dip angle (65°S) of the fault zone observed in the trench (see next section) to estimate the amplitude of the vertical component projected on the fault plane according to the axis defined by the slope of the piercing line (e.g. Nazari et al., 2009). This allows estimating the reverse components along the fault corresponding to 3 successive displacements at 2 ± 0.2 m (average from profiles L1-L1′ and L2-L2′), 4 ± 0.4 m (L3-L3′) and 6 ± 0.6 m (average from profiles L3-L3″ and L4-L4′) (Fig. 9 E), which yields offset amplitude along the slip vector of 4 ± 0.4 m, 8.1 ± 0.8 m, and 12.1 ± 1.2 m.

3.2.2. *Paleoseismological analysis*

To clarify the kinematics of the vertical component along this segment of the Mondy Fault, the amplitude and age of past surface rupturing events, we excavated a trench 4.8 m long, 3 m deep across the

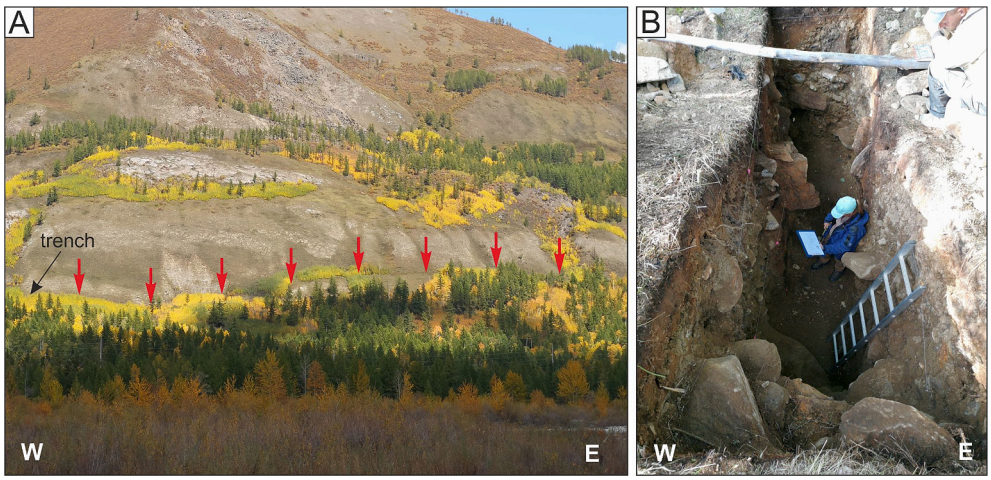

Fig. 8. (A) Northwards view of the Mondy fault scarp (red arrows) in the landscape at site Mondy 2; (B) Photograph of the trench opened at site Mondy 2.

fault scarp (Fig. 8B, see Fig. 4D for location). The trench was open within the fan deposits associated to a temporary stream (51°42.957 N; 100°50.822 E; alt. 1490 m). The fan is composed of clasts of various sizes from gravel to blocks, including well-rounded boulders redeposited from moraines lying higher on the slope (Figs. 8, 10, and Table 3). The deposits have undergone disjunctive deformations, expressed by a chear zone along the main fault zone (unit 70) which shows clearly a reverse component with the thrusting of the southward older unit 60 over the younger northern ones (units 50, 40, 35, 30).

Within the main shear zone, several fractures are identified. They strike N110°E, and dip 60-70° to the south. Within the western wall, fault F1 terminates below unit 10 (modern soil), whereas in the eastern wall the fault seems stopping inside unit 30. We interpret the most recent event horizon (MRE, event 1) post-dating unit 20 and predating unit 10, thus no evidence for it is found in the eastern wall. This may be due to the fact that the deformation on the surface at this point was not brittle, but have produced the folding of unit 20, as evidenced by its concavity. The dating results (Table 4) show that the MRE occurred after 922–1005 cal. years BP.

Bellow MRE horizon, unit 30 is cut by the fault F2, which terminates beneath unit 20. This defines the penultimate event horizon (PE, event 2) (Fig. 10). Taking into account the oldest age obtained from the overlying unit 20 and the youngest sample from the underlying unit 30 (samples MON-20–8 and MON-20–13, respectively), we bracket the age of the PE between 1047 and 5665 cal. years BP.

A pre-penultimate event horizon (PPE, event 3) is interpreted at the base of unit 35 in the eastern wall, and at the base of unit 40 in the western wall, against which fault F3 terminates after having cut through unit 50 (Fig. 10). Since we do not have data about the age of units 35 and 40, the oldest age of unit 30 (5599–5756, sample MON-20–9) was taken as the upper age limit of the PPE. Its lower limit is given by the analysis of sample MON-20–7 in unit 50, which yielded an age of 9009–9293 cal. years BP.

3.2.3. Slip rate, average magnitude and mean recurrence interval of earthquakes

Combining data obtained from the morphotectonic and paleoseismological analyses, we estimate the fault slip rate, average recurrence interval and magnitude of past surface-rupturing earthquakes. The 12.1 ± 1.2 m cumulative slip observed in the morphology that we considered the result of three surface faulting that occurred during the past 9.3 ka allows estimating a maximum slip rate of 1.3 mm/yr, with horizontal and vertical components of 1.1 and 0.7 mm/yr, respectively. Since the Mondy Basin contained a glacier, the edge of which was higher than the surface ruptures at the site Mondy 2, this deformation has a post-glacial age. There are no published data on the age of the moraine located directly above the site Mondy 2. But we can, with some assumptions, use the average age of exposure of boulders collected on the terminal moraine of the Mondy glacier, which is 14 ka (Arzhannikov et al., 2015), as the upper age limit for this cumulative deformation. Thus, we can estimate the minimum slip rate for the Mondy 2 site to be 0.9 mm/yr.The fact that the cumulative offset amplitude along slip vector observed in the morphology (~12 m) is three times larger than the smallest observed offset (~4 m) could be interpreted as the repetition of three similar large surface-rupturing events. The average slip per event of 4 ± 0.4 m yields a mean Moment magnitude of earthquake of M_w 7.4 after Wells and Coppersmith (1994)'s statistical functions. And as already pointed out for the site Mondy 1, this suggest that the. M_w 6.9 1950 Mondy earthquake did not break the surface. Combined with the observations in the trench, these three large events occurred during the past 9.3 ka, which yields a mean recurrence interval comprised between 4.1 and 4.6 ka.

4. Discussion

The morphotectonic and paleoseismological study along the Mondy Fault, within the western margin of the system of basins of Tunka, recognize it as a left-lateral reverse-fault. This result shows that the vertical component along the Mondy Fault has changed from normal to reverse in a recent period of time, as proposed in Larroque et al., 2001 and Arjannikova et al., 2004. This result is also consistent with the left-lateral-reverse fault kinematics that has been recognized along the Sayan and Tunka faults within their relay zone in the eastern margin of the Tunka depression for the Late Pleistocene-Holocene period (Chipizubov and Smekalin, 1999; Sankov et al., 2004, Ritz et al., 2018) (see Fig. 2).

The study of the eastern segment of the Mondy Fault (Mondy 1 site) allowed estimating a maximum slip rate of 1.5 mm/yr over the past ~ 13 ka, while a 0.9–1.3 mm/yr is estimated along the western segment (Mondy 2 site) over the past ~ 9 ka. The horizontal left-lateral slip rate is ~ 1.1 mm/yr for both the eastern and western segments of the fault. It is lower than the left-lateral displacement rates obtained for the Sayan-Tunka fault system within the eastern margin of the Tunka depression, which ranges between 1.3 and 3.9 mm/year (Ritz et al., 2018), and for the Tunka Fault within its central part at 1.5 mm/year (Arzhannikova et al., 2018; Chebotarev et al., 2021). This small deficit along the Mondy Fault can be explained by the fact that the contribution of the vertical displacement component is higher for the Mondy Fault than for the Sayan Fault.. These slip rates values estimated along the Mondy and Tunka faults are in agreement with GPS data obtained within the Baikal-Mongolia region, where a simple deformation model assuming elastic strain accumulation on E-W strike-slip faults shows that the rate of

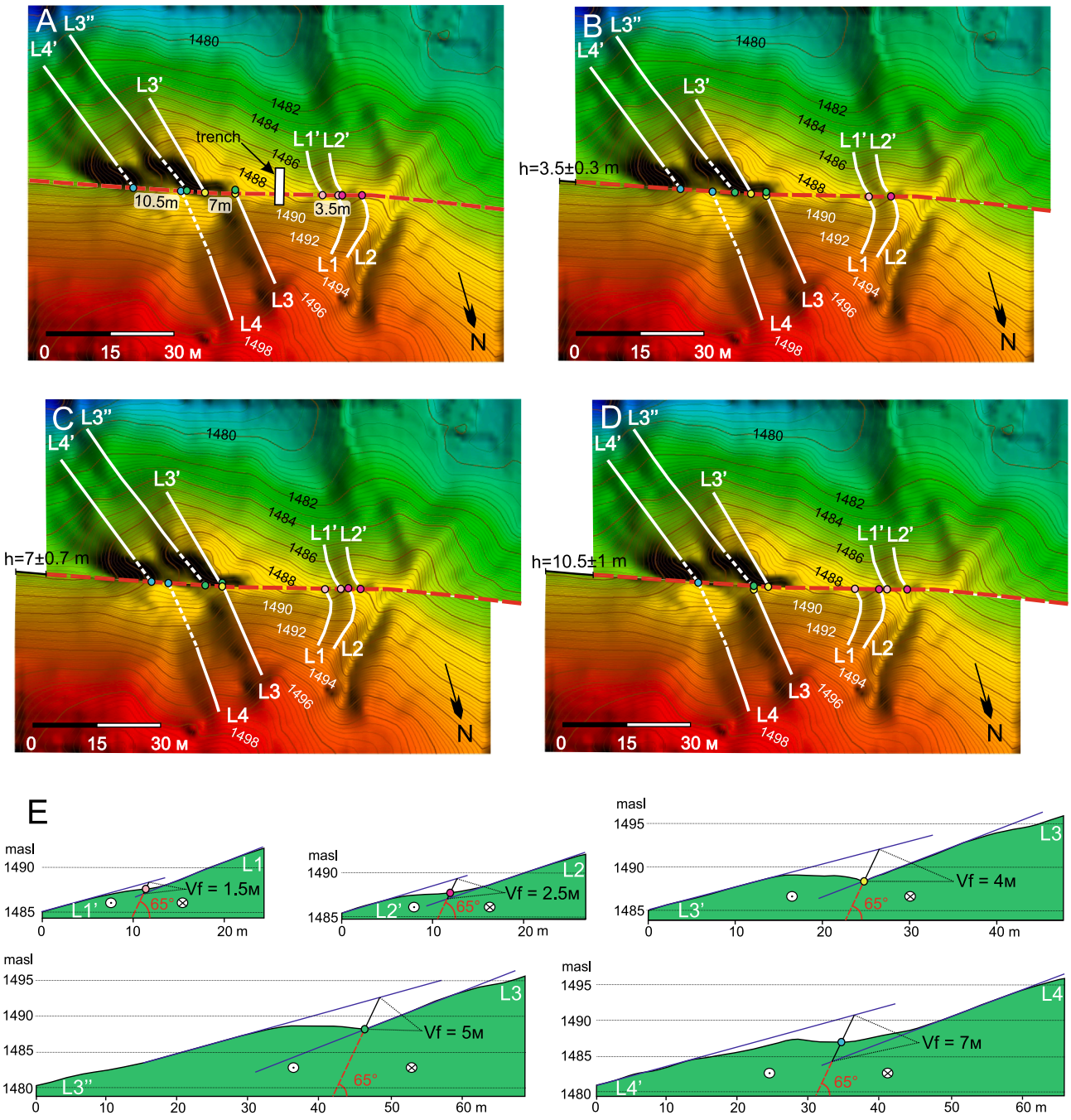

Fig. 9. Digital elevation model (from 1007 topographic points) of the shutter ridge at site Mondy 2 (A) and horizontal component reconstruction before left-lateral displacement of ~ 3.5 m (B), ~7 m (C) and ~ 10.5 m (D) from piercing lines L1-L1′, L2-L2′; L3-L3′ and L3-L3″, L4-L4′, respectively. The isolines indicate the absolute height above sea level in meters (masl). (E) Topographic profiles, reconstructed taking into account the horizontal displacement of ~ 3.5 m (L1-L1′, L2-L2′), ~7 m (L3-L3′) and ~ 10.5 m (L3-L3″, L4-L4′). The Mondy Fault is shown by the red dashed line. h - horizontal offset, Vf - vertical component projected on the fault plane according to the axis defined by the slope of topographic ridge.

horizontal displacement along the Tunka border faults should be of 2 ± 1.2 mm/yr (Calais et al., 2003).

Our results allow also discussing the age of the onset of the kinematics inversion observed within the vertical component, from normal to reverse. Considering that some of the landforms remained preserved in the morphology despite the erosion associated with the glacial periods, we used the cumulative deformations observed along the central segment of the Mondy Fault, within the Khara-Daban interbasin height, such as the large upstream-facing scarps, associated to 300 m left-laterally shifted river riser to estimate the onset of the inversion (Fig. 4A,C, see Fig. 3 for the location). Assuming that the average ~1 mm/year horizontal slip rate that we determined in this work has been constant over the time yields an age ~300 ka for the 300 m total left-lateral displacement observed along the fault. This result is consistent with the minimum age of 140–125 ka, proposed by Arzhannikov et al. (2018) at the eastern margin of the Tunka depression.

In terms of past-earthquakes magnitudes, the morphotectonic and paleoseismological investigations allow estimating an average Moment magnitude of Mw 7.4–7.5 for the past surface-rupturing events that occurred along the fault after Wells and Coppersmith (1994) statistical functions, linking surface displacements and Mw. Still after Wells and Coppersmith (1994), this magnitude would correspond to a surface

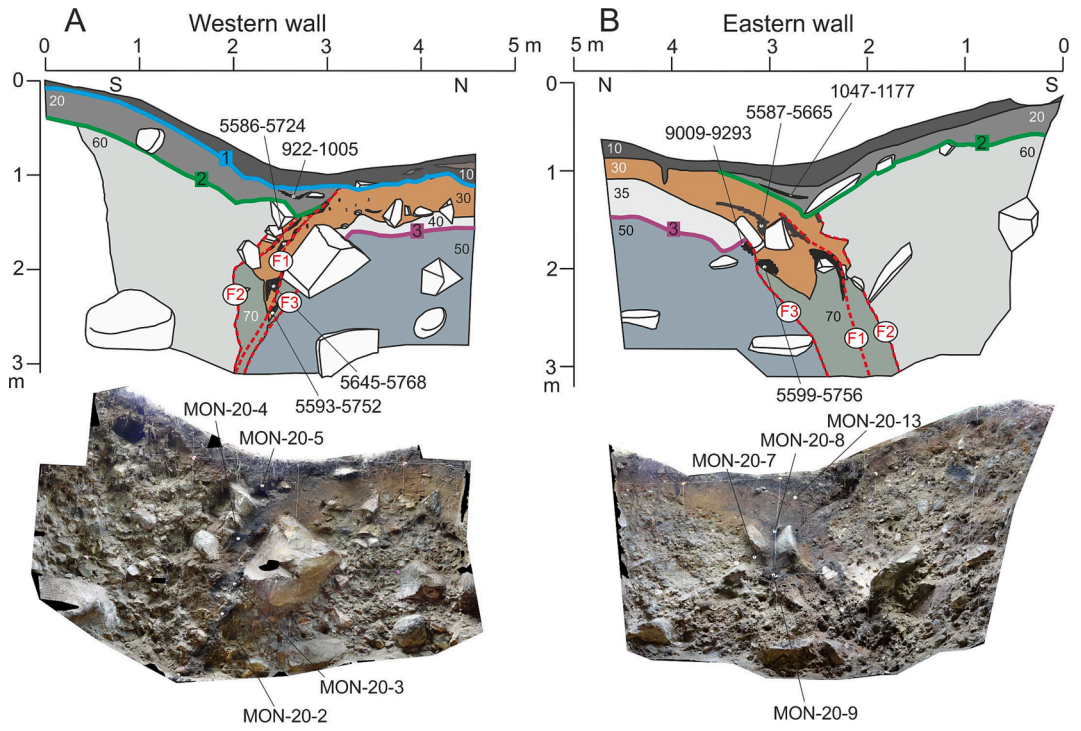

Fig. 10. The stratigraphic log and photo collage of the western (A) and eastern (B) walls of the trench at site Mondy 2. 10–70 - number of units describing in Table 3. White pentagons show the sampling sites for radiocarbon analysis; the calibrated ages (cal years BP) are indicated on the stratigraphic logs, the sample numbers are indicated on the photo collages (Table 4). Red dashed lines show the faults (F1-F3). Bold colored lines show event horizons (1–3).

Table 3
Stratigraphic descriptions for units logged in the trench at site Mondy 2.

Unit	Description of stratigraphy
10	black organic soil
20	dark brown organic-rich clast-supported sandy unit
30	brown sandy-silty unit rich of organic at the upper part, containing charcoals and fragments of angular clasts up to 8 cm
35	greenish-gray clastic unit with poor sub-horizontal stratification. Clasts are sorted, the size of fragments is from 0.5 to 4 cm, with rare inclusions of fragments up to 10 cm, angular or sub-angular. The deposits form a cone, which is exposed in the eastern and northern walls of the trench, and laterally replaced by unit 40 in the western wall
40	greenish-gray sandy matrix, redeposited from unit 35, with angular rock clasts
50	coarse clasts within greenish-gray gravelly-sandy matrix. Clasts are mostly angular with few rounded boulders redeposited from the overlying moraines. The size of clasts is 7–8 cm, with rare inclusions of fragments up to 90 cm
60	loose unsorted angular coarse clasts within greenish-gray gravelly-sandy matrix. The size of fragments is from 1 to 40 cm, with single meter boulders
70	reddish-greenish crushing zone along the main fault. The clasts are crushed to fine gravel with few larger fragments, secondarily oxidized

Table 4
Calculated dates from radiocarbon analysis of paleosoils and charcoals collected in the trench at site Mondy 2. Dendrochronologically calibrated calendar ages were calculated using CALIB 8.2 (Stuiver et al., 2021).

Sample name	Unit number	Lab. no.	14C age year BP	Calibrated age, year BP (2σ)
MON-20–2	70	Poz-134672	4960 ± 40	5593–5752
MON-20–3	30	Poz-134585	5000 ± 40	5645–5768
MON-20–4	30	Poz-134586	4910 ± 40	5586–5724
MON-20–5	20	Poz-134673	1065 ± 30	922–1005
MON-20–7	50	Poz-134685	8190 ± 50	9009–9293
MON-20–8	30	Poz-134761	4910 ± 35	5587–5665
MON-20–9	30	Poz-134748	4980 ± 40	5599–5756
MON-20–13	20	Poz-134752	1180 ± 35	1047–1177

rupture length of about ~ 90 km long, which is the length of the whole Mondy Fault.

The results at the site Mondy 2, suggest that the three past surface-rupturing events had a characteristic slip of ~ 4 m. Assuming also that the ruptures at the site Mondy 1 had characteristic behavior (e.g. Schwartz and Coppersmith, 1984; Sieh, 1996), this yields ~ 4.9 m per event (19.5 m / 4). Although we cannot say this for certain, these results suggest that the Mw6.9 1950 Mondy earthquake did not break the surface, probably due to its large hypocentral depth determined around 14 km (Delouis et al., 2002) (statistically, a Mw 6.9 event would produce surface displacement comprised between 1.2 and 0.9 m (Wells and Coppersmith, 1994)). The 4–5 m displacements values are similar with characteristic slip values observed along other large regional strike-slip faults as the Bulnay and Bogd faults in Mongolia (Kurushin et al., 1998; Ritz et al., 1995; 2006; Rizza et al., 2011; 2015: Kurtz et al., 2018) or the Fu-Yun Fault in Chinese Altay (Klinger et al., 2011). This suggests that active faults in the whole Mongolia-Baikal region correspond to a homogeneous structural domain with a similar inheritance pattern (large inherited deep-seated crustal faults) controlling their quaternary activity.

The average recurrence interval for the surface-rupturing events varies between 3.9 and 4.3 ka and 4.1–4.6 ka for the Mondy 1 and Mondy 2 sites, respectively. Given the size of slip displacements observed in surface suggest that both fault segments – including the one in between (see Fig. 2) - actually broke all together. Those values are similar with recurrence periods of strong earthquakes (3.9–4.2 ka) determined along the eastern Sayan and eastern Tunka faults (Ritz et al., 2018). The distribution of age constraints indicates 4 strong earthquakes associated with all three faults over the past 13.6 ka (Fig. 11). This

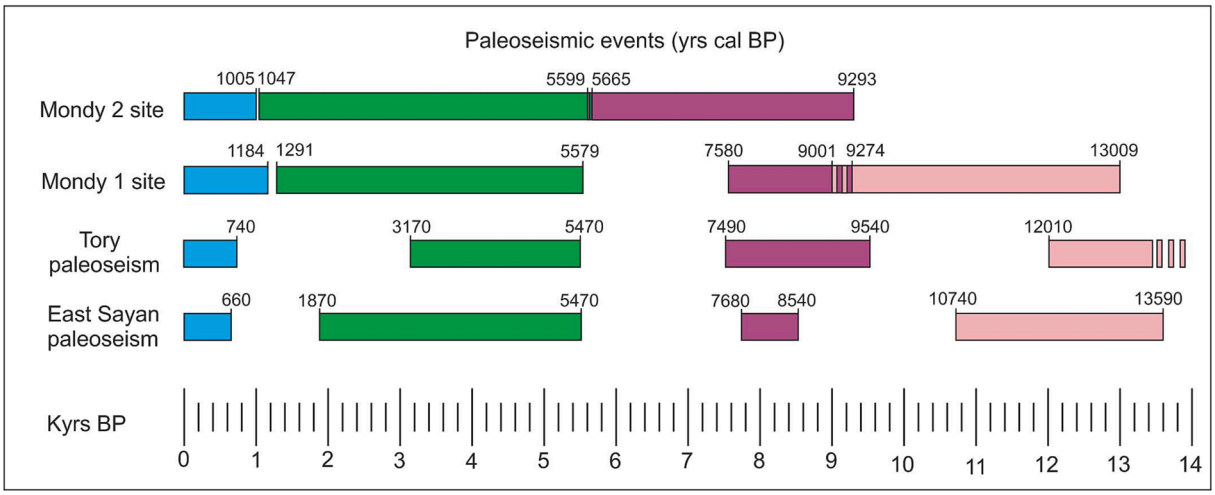

Fig. 11. Age constraints for past surface-rupturing events identified along the Mondy Fault (this study) and comparison with the ages of past-events obtained for the Tory and East Sayan paleoseisms along the eastern segments of the Tunka and Sayan faults, respectively (Chipizubov, Smekalin, 1999; Chipizubov et al., 2003; Ritz et al., 2018). Events that could occur simultaneously along all three faults are highlighted in one color.

suggests that these different faults could have ruptured contemporaneously during regional seismic clusters, as was proposed for the Tunka and Sayan faults (Ritz et al., 2018) and for the Bogd and Bulnay faults (Rizza et al., 2015).

5. Conclusions

The morphotectonic and paleoseismological study brings new insights on Late Pleistocene-Holocene kinematics, slip rate, and seismic potential of the Mondy Fault, one of the large active structure found within the SW Baikal Rift region. We show that the fault has a left-lateral strike-slip kinematics with a strong reverse component, confirming the recent inversion of the tectonic regime on the southwestern Baikal Rift region in the Late Pleistocene-Holocene period. On the basis of remote sensing analysis and detailed geomorphological mapping we also recognized that the Mondy Fault is composed of three segments. The segment boundaries can be violated by the ruptures as suggested by paleoseismology.

The combination of the morphotectonic and paleoseismological observations allows estimating a slip rate along the Mondy Fault of 0.9–1.5 mm/yr over the past ~ 13 ka, and identifying 4 large surface-rupturing events with Moment magnitude 7.4–7.5, having occurred with an average recurrence interval of ~ 4 ka. This interval coincides with the mean recurrence interval of strong surface-rupturing events observed along the eastern sections of the Tunka and Sayan faults (Ritz et al., 2018). Moreover, the consistency of the paleoearthqukes age ranges for the three faults suggests that they may have ruptured during seismic clusters. These results reinforce the conclusion that the faults within the Tunka depression represent a strong seismic hazard for the region, in particular for the densely populated Irkutsk agglomeration.

CRediT authorship contribution statement

A.V. Arzhannikova: Conceptualization, Methodology, Investigation, Validation, Writing – original draft. **S.G. Arzhannikov:** Methodology, Investigation, Software. **J.-F. Ritz:** Supervision, Methodology, Validation. **A.A. Chebotarev:** Investigation, Visualization. **A.S. Yakhnenko:** Investigation, Formal analysis.

Declaration of Competing Interest

The authors declare that they have no known competing financial interests or personal relationships that could have appeared to influence the work reported in this paper.

Data availability

No data was used for the research described in the article.

Acknowledgments

The field study of the Mondy 1 site was supported by Russian Foundation for Basic Research and CNRS (PRC program, grant № 20-55-15002/PRC 297213). The field study of the Mondy 2 site and final interpretation of the results was supported by the Russian Science Foundation (grant № 22-17-00049). Remote sensing analysis of morphotectonic features was done thanks to the TanDEM-X project DEM_GEOL1193. The radiocarbon samples were analyzed at the Poznan Radiocarbon Laboratory and at the French National Platform LMC14 of the National Service of INSU "ARTEMIS" for the radiocarbon dating. The work was conducted using equipment and infrastructure of the Centre for Geodynamics and Geochronology at the Institute of the Earth's Crust, Siberian Branch of the Russian academy of Sciences (grant no 075-15-2021-682). We thank Volodymyr Vasyliev for his help in the field work. We thank Dr. Daniela Pantosti and anonymous reviewer for their thorough reviews which helped to improve the manuscript.

References

Arjannikova, A., Larroque, C., Ritz, J.-F., Déverchère, J., Stéphan, J.F., Arjannikov, S., San'kov, V., 2004. Geometry and kinematics of recent deformation in the Mondy-Tunka area (south-westernmost Baikal Rift zone, Mongolia-Siberia). Terra Nova 16 (5), 265–272.

Arzhannikov, S.G., Braucher, R., Jolivet, M., Arzhannikova, A.V., 2015. Late Pleistocene glaciations in southern East Sayan and detection of MIS 2 terminal moraines based on beryllium (10Be) dating of glacier complexes. Russ. Geol. Geophys. 56, 1509–1521.

Arzhannikov, S.G., Ivanov, A.V., Arzhannikova, A.V., Demonterova, E.I., Jansen, J.D., Preusser, F., Kamenetsky, V.S., Kamenetsky, M.B., 2018. Catastrophic events in the Quaternary out flow history of Lake Baikal. Earth Sci. Rev. 177, 76–113.

Arzhannikova, A.V., Arzhannikov, S.G., Semenov, R.M., Chipizubov, A.V., 2005. Morphotectonics and late Pleistocene - Holocene deformations in the Tunka system of basins (Baikal Rift, Siberia). Z. Geomorphol. 49 (4), 485–494.

Arzhannikova, A., Arzhannikov, S., Braucher, R., Jolivet, M., Aumaître, G., Bourlès, D., Keddadouche, K., 2018. Morphotectonic analysis and 10Be dating of the Kyngarga river terraces (southwestern flank of the Baikal rift system, South Siberia). Geomorphology 303, 94–105.

Arzhannikova, A.V., Larroque, C., Arzhannikov, S.G., 2003. Holocene deformation in the western end of the Tunka system of rift basins (Southwestern Baikal Rift). Russ. Geol. Geophys. 44 (4), 373–379.

Arzhannikova, A.V., Melnikova, V.I., Radziminovich, N.A., 2007. Late Quaternary and current deformation in the western Tunka system of basin: evidence from structural geomorphology and seismology. Russ. Geol. Geophys. 48, 305–311.
Arzhannikova, A., Ritz, J.-F., Larroque, C., Antoine, P., Arzhannikov, S., Chebotarev, A., Stéphan, J.-F., Massault, M., Michelot, J.-L., 2020. Cryoturbation versus tectonic deformation along the southern edge of the Tunka Basin (Baikal Rift System), Siberia: New insights from morphotectonic and stratigraphic analyses. J. Asian Earth Sci. 204, 104569.
Calais, E., Vergnolle, M., San'kov, V., Lukhnev, A., Miroshnitchenko, A., Amarjargal, S., Déverchère, J., 2003. GPS measurements of crustal deformation in the Baikal-Mongolia area (1994–2002): Implications for current kinematics of Asia. J. Geophys. Res. Solid Earth 108 (B10), 2501.
Calais, E., Dong, L., Wang, M., Shen, Z., Vergnolle, M., 2006. Continental deformation in Asia from a combined GPS solution. Geophys. Res. Lett. 33, L24319. https://doi.org/10.1029/2006GL028433.
Chebotarev, A., Arzhannikova, A., Arzhannikov, S., 2021. Long-term throw rates and landscape response to tectonic activity of the Tunka Fault (Baikal Rift) based on morphometry. Tectonophysics 810, 228864.
Chipizubov, A.V., Smekalin, O.P., 1999. Fault scarps and the causative prehistoric earthquakes in the main Sayan fault zone. Russ. Geol. Geophys. 40 (6), 921–931.
Chipizubov, A.V., Smekalin, O.P., Semenov, R.M., 2003. Fault scarps and prehistoric earthquakes in the Tunka fault (southwestern Baikal region). Russ. Geol. Geophys. 44 (6), 587–602.
Delouis, B., Der'verche're, J., Melnikova, V., Radziminovitch, N., Loncke, L., Larroque, C., Ritz, J.F. and San'kov, V., 2002. A reappraisal of the 1950 (Mw 6.9) Mondy earthquake, Siberia, and its relationship to the strain pattern at the south-western end of the Baikal rift zone. Terra Nova 14, 491–500.
Doser, D., 1991. Faulting within the western Baikal rift as characterized by earthquake studies. Tectonophysics 196, 87–107.
Filippova, A.I., Bukchin, B.G., Fomochkina, A.S., Melnikova, V.I., Radziminovich, Y.B., Gileva, N.A., 2022. Source process of the September 21, 2020 Mw 5.6 Bystraya earthquake at the South-Eastern segment of the Main Sayan fault (Eastern Siberia, Russia). Tectonophysics 822, 229162.
Jolivet, M., De Boisgrollier, T., Petit, C., Fournier, M., Sankov, V.A., Ringenbach, J.-C., Byzov, L., Miroshnichenko, A.I., Kovalenko, S.N., Anisimova, S.V., 2009. How old is the Baikal Rift Zone? Insight from apatite fission track thermochronology. Tectonics 28, TC3008. https://doi.org/10.1029/2008TC002404.
Jolivet, M., Arzhannikov, S., Chauvet, A., Arzhannikova, A., Vassallo, R., Kulagina, N., Akulova, V., 2013. Accomodating large-scale intracontinental extension and compression in a single stress-field: A key example from the Baikal Rift System. Gondw. Res. 24 (3–4), 918–935.
Klinger, Y., Etchebes, M., Tapponnier, P., Narteau, C., 2011. Characteristic slip for five great earthquakes along the Fuyun fault in China. Nat. Geosci. 4 (6), 389–392. https://doi.org/10.1038/ngeo1158.
Kurtz, R., Klinger, Y., Ferry, M., Ritz, J.-F., 2018. Horizontal surface-slip distribution through several seismic cycles: the Eastern Bogd fault, Gobi-Altai, Mongolia. Tectonophysics 734, 167–182. https://doi.org/10.1016/j.tecto.2018.03.011.
Kurushin, R.A., Bayasgalan, A., Olziybat, M., Enhtuvshin, B., Molnar, P., Bayarsayhan, C., Hudnut, K.W., Lin, J., 1998. The surface rupture of the 1957 Gobi-Altay, Mongolia, earthquake. Geol. Soc. Am. Spec. Pap. 320, 144. https://doi.org/10.1130/0-8137-2320-5.1.
Larin, S.I., 2019. Glacial-nival morpholithogenesis of the Tunka rift in the late Pleistocene and Holocene. In: Rasskazov, S.V., Primina, S.P. (Eds.), Rifting, orogenesis, and accompanied processes. Proceedings of the IVth All-Russian symposium with participation of foreign scientists, dedicated to the 90th anniversary of Academician Nikolay Logachev. Institute of the Earth's Crust SB RAS, Irkutsk, pp. 89-91.
Larroque, C., Ritz, J.F., Stéphan, J.F., San'kov, V., Arjannikova, A., Calais, E., Deverchère, J., Loncke, L., 2001. Interaction compression-extension à la limite Mongolie–Sibérie: analyse préliminaire des déformations récentes et actuelles dans le bassin de Tunka. C.R. Acad. Sci. Paris 332, 177–184.
Liu, X., Xu, W., Radziminovich, N.A., Fang, N., Xie, L., 2022. Transtensional coseismic fault slip of the 2021 Mw 6.7 Turt Earthquake and heterogeneous tectonic stress surrounding the Hovsgol Basin, Northwest Mongolia. Tectonophysics 836, 229407.
Lukhnev, A.V., San'kov, V.A., Miroshnichenko, A.I., Ashurkov, S.V., Calais, E., 2010. GPS rotation and strain rates in the Baikal-Mongolia region. Russ. Geol. Geophys. 51, 785–793.
Lukina, N.V., 1989. Quaternary motions on faults in the southwestern flank of the Baikal rift system. Geotectonika 2, 89–100.
Lunina, O.V., Andreev, A.V., Gladkov, A.S., 2015. The 1950 Mw = 6.9 Mondy earthquake in southern East Siberia and associated deformations: facts and uncertainties. J. Seismol. 19 (1), 171–189.
Lunina, O.V., Gladkov, A.S., 2004. Fault structure of the Tunka rift as a reflection of oblique extension. Dokl. Earth Sci. 398 (7), 928–930.
Lunina, O.V., Gladkov, A.S., Afonkin, A.M., Serebryakov, E.V., 2016. Deformation style in the damage zone of the Mondy fault: GPR evidence (Tunka basin, southern East Siberia). Russ. Geol. Geophys. 57, 1269–1282.
Maksimov, E.V., 1965. On the origin of the terraces of the Mondy Basin in East Sayan. Izv. VGO 97 (4), 370–373.
McCalpin, J.P., Khromovskikh, V.S., 1995. Holocene paleoseismicity of the Tunka fault, Baikal rift. Russia. Tectonics 14 (3), 594–605.
Melnikova, V. I., Radziminovich, N. A. & Adyaa, M., 2004. Mechanisms of earthquake foci and seismotectonic deformations of the Mongolia region. In: Dzhurik, V.I. & Dugarmaa, T. (Eds.), Complex geophysical and seismological investigations in Mongolia. Ulaan-Baatar – Irkutsk, pp. 165-170.
Nazari, H., Ritz, J-F., Shafei, A., Ghassemi, A., Salamati, R., Michelot, J-L. and Massault, M., 2009. Morphological and paleoseismological analyses of the Taleghan fault, Alborz, Iran. Geophys. J. Int. 178, 1028-1041. doi: 10.1111/j.1365-246X.2009.04173.x.
Parfeevets, A.V., San'kov, V.A., 2006. Geodynamic conditions of evolution of the Tunka branch in the Baikal Rift system. Geotectonics 5, 377–398.
Petit, C., Déverchère, J., 2006. Structure and evolution of the Baikal rift: a synthesis. Geochem. Geophys. Geosyst. 7, Q11016.
Petit, C., Fournier, M., 2005. Present-day velocity and stress fields of the Amurian Plate from thin-shell finite-element modelling. Geophys. J. Int. 160 (1), 357–369.
Petit, C., Déverchère, J., Houdry, F., San'kov, V.A., Melnikova, V.I., Delvaux, D., 1996. Present-day stress field changes along the Baikal rift and tectonic implications. Tectonics 15, 1171–1191.
Radziminovich, N.A., 2021. Focal mechanisms of earthquakes of southern Baikal region and Northern Mongolia. Geodynam. Tectonophys. 12 (4), 902–908.
Radziminovich, N.A., Gileva, N.A., Melnikova, V.I., Ochkovskaya, M.G., 2013. Seismicity of the Baikal rift system from regional network observations. J. Asian Earth Sci. 62, 146–161.
Radziminovich, N.A., Bayar, G., Miroshnichenko, A.I., Demberel, S., Ulziibat, M., Ganzorig, D., Lukhnev, A.V., 2016. Focal mechanisms of earthquakes and stress field of the crust in Mongolia and its surroundings. Geodynamics & Tectonophysics 7 (1), 23–38.
Ritz, J.-F., Brown, E.T., Bourlès, D.L., Philip, H., Schlupp, A., Raisbeck, G.M., Yiou, F., Enkhtuvshin, B., 1995. Slip rates along active faults estimated with cosmic-ray-exposure dates: Application to the Bogd fault, 20 Gobi-Altaï, Mongolia. Geology 23, 1019–1022.
Ritz, J.-F., Arzhannikova, A., Vassallo, R., Arzhannikov, S., Larroque, C., Michelot, J.-L., & Massault, M., 2018. Characterizing the present-day activity of the Tunka and Sayan faults within their relay zone (western Baikal rift system, Russia). Tectonics 37 (5), 1376–1392. https://doi.org/10.1002/2017TC004691.
Ritz, J.-F., Larroque, C., Stéphan, J.F., Sankov, V., Arjannikova, A., Calais, E., Deverchère, J., Loncke, L., 2000. In: When compression meets extension: Interaction or competition? The example of the Tunka basin (Western Baikal, Siberia). University of Manchester, p. 122.
Ritz, J.-F., Vassallo, R., Braucher, R., Brown, E.T., Carretier, S., Bourlès, D.L., 2006. Using in situ produced ^{10}Be to quantify active tectonics in the Gurvan Bogd mountain range (Gobi-Altay, Mongolia). Geol. Soc. Am. 415, 87–110.
Rizza, M., Ritz, J-F., Prentice, C., Vassallo, R., Braucher, R., Larroque, C., Arzhannikova, A., Arzhannikov, S., Mahan, S., Massault, M., Michelot, J.-L., Todbileg, M., ASTER Team, 2015. Earthquake geology of the Bolnay fault (Mongolia). Bulletin of Seismological Society of America 105 (1), 72-93. doi: 10.1785/0120140119.
Rizza, M., Ritz, J.-F., Braucher, R., Vassallo, R., Prentice, C., Mahan, S., McGill, S., Chauvet, A., Marco, S., Todbileg, M., et al., 2011. Slip rate and the slip magnitude of past earthquakes along the Bogd left-lateral strike-slip fault (Mongolia). Geophys. J. Int. 186, 897–927. https://doi.org/10.1111/j.1365-246X.2011.05075.x.
Sankov, V.A., Chipizubov, A.V., Lukhnev, A.V., Smekalin, O.P., Miroshnichenko, A.I., Calais, E., Déverchère, J., 2004. Assessment of a large earthquake risk in the zone of the main Sayan fault using GPS geodesy and paleoseismology. Russ. Geol. Geophys. 45 (11), 1369–1376.
Sankov, V.A., Lukhnev, A.V., Miroshnichenko, A.I., Ashurkov, S.V., Byzov, L.M., Dembelov, M.G., Calais, E., Déverchère, J., 2009. Extension in the Baikal rift: present-day kinematics of passive rifting. Dokl. Earth Sci. 425 (2), 205–209.
Sankov, V.A., Lukhnev, A.V., Miroshnitchenko, A.I., Dobrynina, A.A., Ashurkov, S.V., Byzov, L.M., Dembelov, M.G., Calais, E., Déverchère, J., 2014. Contemporary horizontal movements and seismicity of the south Baikal basin (Baikal rift system). Izv. Phys. Solid Earth 50 (6), 785–794.
Schwartz, D.P. and Coppersmith, K.J., 1984. Fault Behavior and Characteristic Earthquakes: Examples From the Wasatch and San Andreas Fault Zones. Journal of geophysical research 89, B7, 5681-5698.
Shchetnikov, A., 2017. Morphotectonic inversion in the Tunka rift basin (southwestern Baikal region). Russ. Geol. Geophys. 58 (7), 778–786.
Sieh, K., 1996. The repetition of large-earthquake ruptures. Proceedings Natl. Acad. Sci. USA 93, 3764–3771.
Smekalin, O.P., Shchetnikov, A.A., White, D., 2013. Arshan palaeoseismic feature of the Tunka fault (Baikal rift zone, Russia). J. Asian Earth Sci. 62, 317–328.
Stuiver, M., Reimer, P.J., and Reimer, R.W. 2021. CALIB 8.2 [WWW program]. http://calib.org.
Treskov, A.A., Florensov, N.A., 2006. The Mondy earthquake of 4 (5) April 1950: Preliminary report. In: Potapov, V.A. (Ed.), Andrei Alekseevich Treskov. IZK, Irkutsk, pp. 166–188 in Russian.
Wells, D.L., Coppersmith, K.J., 1994. Empirical relationships among magnitude, rupture length, rupture area, and surface displacement. Bull. Seismol. Soc. Am. 84, 974–1002.